Supporting Information

Single Atomic Fe-Pyridine N Catalyst with Dense Active Sites Improve Bifunctional Electrocatalysts Activity for Rechargeable and Flexible Zn-Air Battery

Wenhui Deng[a], *Tianjing Wu*[a,*], *Yufeng Wu*[a], *Haitao Zheng*[a], *Guang Li*[a], *Meixia Yang*[a], *Xiaoqing Zou*[a], *Yansong Bai*[a], *Yingchang Yang*[b], *MingJun Jing*[a,*], *Xianyou Wang*[a]

W. Deng, Prof. T. Wu, Y. Wu, H. Zheng, G, Li, M. Xia, Prof. X. Zou, Prof. Y. Bai, Prof. Y. Yang, Prof. M. Jing, and Prof. X. Wang
National Base for International Science & Technology Cooperation, National Local Joint Engineering Laboratory for Key Materials of New Energy Storage Battery, Key Laboratory of Environmentally Friendly Chemistry and Application of Ministry of Education, College of Chemistry
Xiangtan University
Xiangtan, 411105, China
E-mail: twu@xtu.edu.cn; jingmingjun86@163.com

Prof. Y. Yang
College of Material and Chemical Engineering
Tongren University
Tongren, 554300, China

Table of contents

Section S1. Experimental section.

1.1 Chemicals.

Azodiisobutyronitrile (AIBN), Ammonium persulphate (APS), Anhydrous ferric chloride ($FeCl_3$), and Zinc chloride dihydrate ($ZnCl_2$) are provided via Sinopharm Chemical Reagent Co., Ltd. (Shanghai, China). Pt/C (20 wt%) is purchased from Sigma-Aldrich Chemical Regent Co., Ltd. Pyrrole, Aniline, 2-Vinyl-Pyridine, and IrO_2 are obtained from Energy Chemical Co., Ltd. Nafion (5%) is originate from DuPont. Other reagents are provided by a Chemical company and used without further purification. Deionized water was used in all the experiments.

1.2 Sample preparation.

Synthesis of NC-1: A 2 mL portion of 2-Vinyl-Pyridine is taken into a test tube (10 mL). Then, anhydrous tetrahydrofuran (1 mL) and AIBN (0.8 mL, 0.02 g mL^{-1}) are added as a solvent and oxidizing agent into a Pyrex tube (10 mL), followed through three freeze-pump-thaw cycles. The tube is sealed off under vacuum and stirred at 70 °C for 4 h. Then, the THF (5 mL) is poured into the product, and the mixture is added dropwise to the N-hexane (200 mL) under vigorous stirring.[1] The yellow precipitate is collected by filtering and washed with N-hexane carefully. The yellow solid is dried at 60 °C under a vacuum oven. The compound is carbonized at 800 ℃ for 3 h with a 3 ℃ min^{-1} ramp rate under an Ar atmosphere to obtain NC-1.

Synthesis of NC-2: The polyaniline (PANI) precursor with block morphology is synthesized via an oxidative polymerization. 2 mL aniline monomer in a 1 M HCl aqueous solution is oxidized at 0 - 5 ℃ for 24 h. In this system, 1.6 g APS is used as

an oxidizing agent. The product is washed using dilute HCl solution (1 M) and deionized water until the filtrate is colorless and neutral.[2] The sample of PANI is subjected to pyrolysis under Ar flow at 800 °C for 3 h to yield the NC-2.

Synthesis of NC-3: In the synthetic process, 1.6 g of APS is dissolved in 240 mL dilute hydrochloric acid (HCl) solution (1 M) at 0 - 5 ℃ using a stirrer for 10 min to form a homogenous dispersion. After water bath temperature at low 5 ℃, 2 mL pyrrole is injected into the above solution under vigorous stirring for 10 min. Then, the reaction is maintained for 24 h without stirring at 0 - 5 ℃. The black PPY nanoparticles are filtered and washed with dilute HCl solution (1 M) and deionized water. The as-prepared PPY nanoparticles are dried overnight at 60 ℃ under a vacuum oven.[3] To synthesize NC-3, PPY is directly heated to 800 °C at a heating rate of 3 °C min^{-1}, and the target temperature is maintained in an argon atmosphere for 3 hours.

Synthesis of Fe/Fe-NC-3, Fe-NC-3, and Zn-NC-3: A mixture of $FeCl_3$ and PPY nanoparticles (mass ratio = 10 : 1) is placed in an agate mortar and quickly ground. The black powder mixture is pyrolyzed at 800 °C for 3 h under Ar gas conditions with 3 °C min^{-1}. Then, the obtained product is re-dispersed in 60 mL HCl (1 M) at 50 ℃ for 6 h to remove inactive and unstable Fe species. The sample Fe/Fe-NC-3 is washed with deionized water until neutrality (PH = 7) and finally dried in a vacuum overnight. A comparative sample with a concentration of HCl (4 M) is prepared in the same method and the resultant product is denoted as Fe-NC-3. The PPY nanoparticles are treated with $ZnCl_2$ by the same procedure named Zn-NC-3.

2.3 Characterizations.

The microstructure of as-synthesized materials is analyzed via the Scanning electron microscope (Zeiss Sigma 300), which is accelerated voltage of 5 kV. The internal structure and elemental distribution of the as-prepared materials are identified by transmission electron microscopy (TEM, JEM-2100F) operating at 200 kV, and their crystallinity is collected using an X-ray diffractometer (XRD) utilizing Cu-kα radiation (D8 DISCOVER diffractometer). Nitrogen adsorption-desorption isotherms are performed through the Brunauer-Emmet-Teller analysis (TriStar II 3020 2.00). The chemical compositions of the catalysts are analyzed using X-ray photoelectron spectroscopy (XPS, ESCALAB250Xi) and Fourier transforms infrared (FT-IR) spectroscopy is carried out using a Thermo Scientific Nicolet 6700. The Raman spectrum is collected using a Raman spectrometer (Renishaw InVia system) with an excitation wavelength of 532 nm.

2.4. Electrochemical measurements.

The electrocatalytic measurements are conducted on a rotating ring-disk electrode (ATA-1B) connected to a CHI660 electrochemical workstation (Chen Hua, Shanghai, China) at room temperature. CV and RDE measurements are conducted using a typical three-electrode system, which is composed of an Ag/AgCl (saturated KCl electrolyte) as the reference electrode, a platinum web as the counter electrode, and glassy carbon ($S = 0.0706\ cm^{-2}$) or carbon paper ($S = 0.25\ cm^{-2}$) as the working electrode. 2.5 mg catalyst is dispersed in 475 μL ethanol solution and 25 μL 5 wt% Nafion and then ultrasonic treatment for 30 min. The 10 μL of catalyst ink is dropped onto a glassy

carbon electrode with a mass loading of 0.71 mg cm^{-2} for the ORR test, and a 50 μL portion of the catalyst ink is spread on a carbon paper working electrode with the loading of 1.0 mg cm^{-2} for the OER measurement. For comparison, the commercial Pt/C and IrO_2 catalyst ink is also prepared using the same method. All potential is replaced with RHE ($E_{RHE} = E_{Ag/AgCl} + 0.0592\ pH + 0.197\ V$). The CV curves are scanned at 50 mV s^{-1} and examined environment in O_2/N_2-saturated 0.1 M KOH from 0.2 to 1.2 V. The double-layer capacitance (C_{dl}) is tested in non-faradic potential (1.0 - 1.2 V) with different scan rates from 10 to 50 mV s^{-1}. For the ORR performance measurements, the LSV curves are performed in an O_2-saturated at varying rotating rates from 400 to 2000 rpm at a rate of 5 mV s^{-1}. The OER activity is carried out in O_2-saturated 1 M KOH electrolyte with a scan rate of 5 mV s^{-1} (voltage ranging from 1.2 - 2.0 V). The chronoamperometry tests at 1600 rpm are examined for the stability and methanol durability of the catalyst.

The electron transfer number (n) is calculated by the Koutecky-Levich equation in the diffusion-limiting densities (J_L) of the potential region:

$$\frac{1}{J} = \frac{1}{J_L} + \frac{1}{J_K} = \frac{1}{B\sqrt{\omega}} + \frac{1}{j_K} \quad (1)$$

$$B = 0.62nFC_0(D_0)^{2/3}v^{1/6} \quad (2)$$

Where J, J_L, and J_K are assigned the measured total current density, diffusion-limiting, and kinetic current density (mA cm^{-2}), respectively. ω represents rpm. F is the Faraday constant ($F = 96485\ C\ mol^{-1}$). The dissolved concentration of O_2 is got C_0 (1.2×10^{-3}

mol l^{-1}) in 0.1 M KOH solution. D_0 is the diffusion co-efficient of O_2 ($D_0 = 1.9 \times 10^{-5}$ cm^2 s^{-1}). ν is the kinetic viscosity for electrolyte (7×10^{-2} cm^2 s^{-1}).

2.5. Zn-air battery assembly.

The measurements of home-made Zn-air batteries are tested using a two-electrode system. Dispersing the as-prepared catalyst ink is dripped to the carbon cloth as the air cathode (catalyst loading is 2.5 mg cm^{-2}). A polished zinc plate is used as the anode. The 6.0 M KOH solution contained 0.2 M zinc acetate is employed as an electrolyte. The measurements are performed by the CHI-660E electrochemical workstation and LAND CT2001A instrument.

2.6. All-solid-state Zn-air battery assembly.

The structure of the flexible solid Zn-air batteries is constructed using a polished zinc plate as the anode, Polyvinyl alcohol (PVA) as the solid electrolyte, and the as-prepared catalysts loaded on carbon cloth as air electrodes. The synthesis procedure of gel polymer electrolyte is as follows. Firstly, 4 g PVA is added to 40 mL distilled water at 95 °C to form a homogeneous solution (about stirring 1 h). Next, 4 mL 18 M KOH with 0.2 M zinc acetate is slowly added to PVA the solution with continuous stirring (40 min). The mixture is poured into the mold at -20 °C for 12 h.[4] Finally, the clean zinc foil and air cathode are located on both sides of the PVA electrolyte and PET sheet package to form a sandwich-like the all-solid-state Zn-air battery.

Section S2: Material characterizations.

2.1 SEM and TEM characterizations.

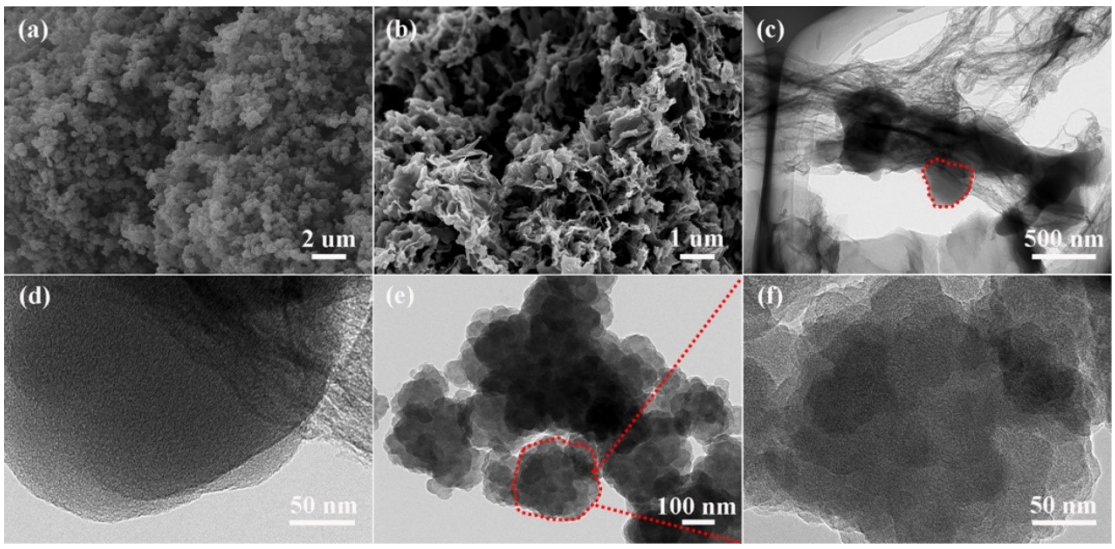

Figure S1. (a, b) SEM image of Zn-NC-3 and Fe-NC-3. (c-f) TEM image of Zn-NC-3 and Fe-NC-3.

The SEM result proves that Zn-NC-3 remains similar in morphology to NC-3 without obvious structural deterioration (Figure S1a). The Fe-NC-3 displays a 3D network structure, which provides abundant active sites and a large contact area between catalyst and electrolyte/air for enhanced electrocatalytic performance. (Figure S1b). TEM image of Fe-NC-3 (Figure S1c, d) indicates a few carbon nanoparticles without whole conversion to a 3D porous structure and shows no appearance of lattice fringes, suggesting the complete removal of Fe species and the damage of structure. As revealed in Figure S1e, f, the internal structure of the NC-3 exhibits a solid nanosphere.

2.2 XRD and Raman characterizations.

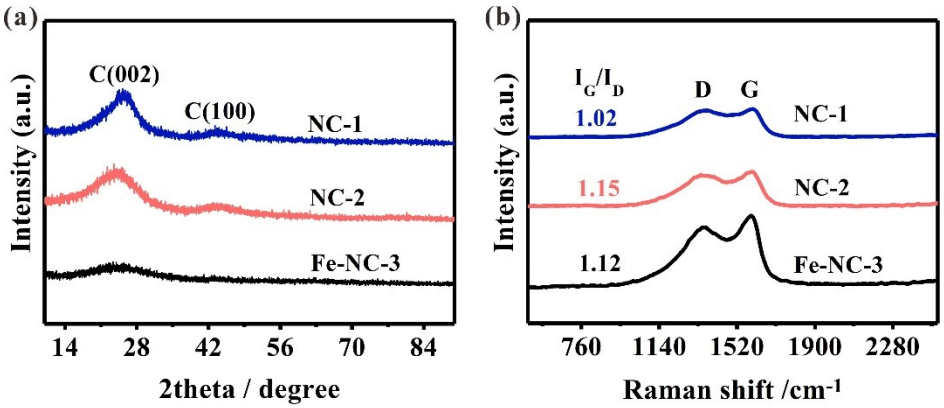

Figure S2. (a) XRD patterns and (b) Raman spectra of NC-1, NC-2, and Fe-NC-3.

The highly graphitic degree of the as-prepared catalysts is confirmed by the XRD and Raman spectroscopy. As confined in Figure S2a, the sample catalysts present two broad peaks at 27.7° and 43.2° corresponding to the (002) and (100) lattice planes of the carbon structure. Except for the two graphitized carbon peaks, no other diffraction peaks ascribed to Fe species are observed, suggesting no highly crystalline Fe species in the Fe-NC-3 material, which is treated with a high concentration of acid. Raman spectra for Fe-NC-3 show two peaks at 1347 and 1572 cm^{-1} with the I_G/I_D value of 1.12 (Figure S2), larger than that of NC-3 (I_G/I_D = 1.11), demonstrating a high graphitic degree of the carbon substrate.

2.3 XPS spectra for NC-3, Fe/Fe-NC-3, and Fe-NC-3.

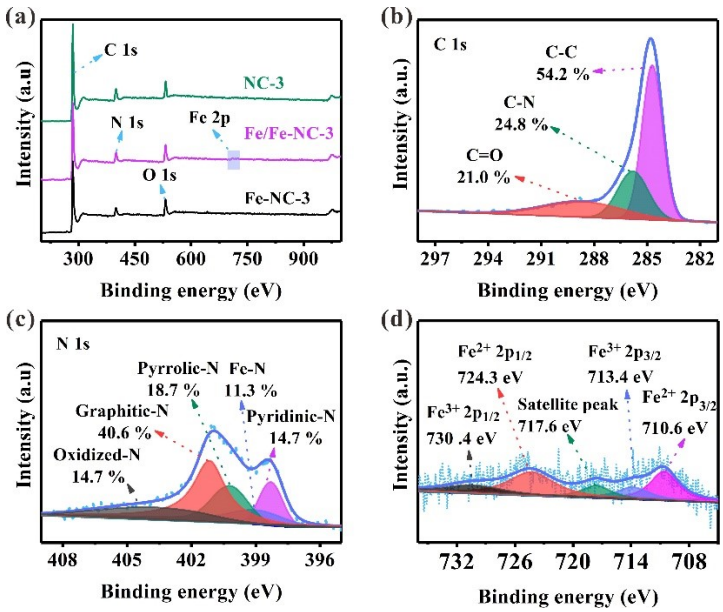

Figure S3. (a) The XPS full spectra of NC-3, Fe/Fe-NC-3, and Fe-NC-3. (b) High-resolution C 1s XPS spectra of NC-3. (c) High resolution XPS spectrum of N 1s and Fe 2p for Fe-NC-3.

The C 1s, N 1s, O 1s, and Fe 2p signals are detected in the XPS survey spectra for NC-3, Fe/Fe-NC-3, and Fe-NC-3 (Figures S3a). Additional peaks for Fe 2p can be observed in Fe/Fe-NC-3, indicating the successful introduction of Fe atoms. The wide XPS spectra of the Fe-NC-3 no a Fe 2p peak due to the scarcity of Fe element. The high-resolution C 1s spectrum for NC-3 is deconvoluted into the three different peaks in Figure S3b, located at C-C (284.7 eV), C-N (285.4 eV), and C=O (289.0 eV)[5], respectively. By contrast Fe/Fe-NC-3, the Fe-NC-3 catalyst is observed the concentration for Oxidized-N increases from 12.1 to 14.7 %, demonstrating the elimination of active sites. And the Fe-NC-3 no obvious metallic Fe or FeC_x signal can be fitted.

Section S3 Electrochemical characterizations.

3.1 CV curves of the carbon materials, Zn-NC-3, and Fe-NC-3.

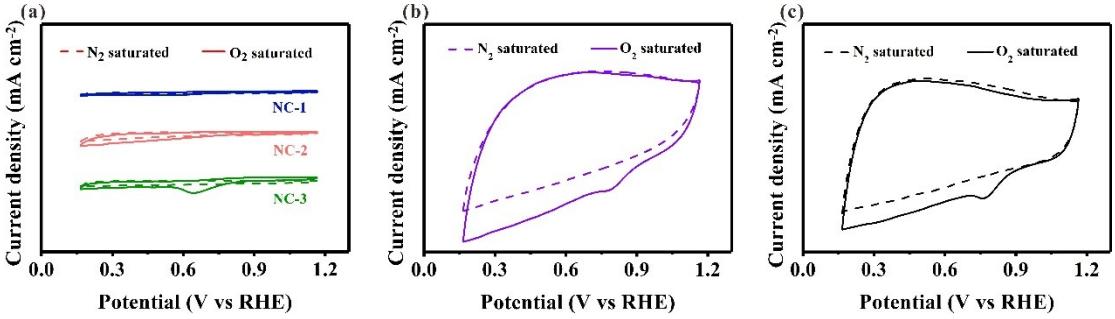

Figure S4. CV curves of NC-1, NC-2, and NC-3 (a), Zn-NC-3 (b), and Fe-NC-3 (c).

The CV profile reveals that no cathodic peak appeared in the N_2-saturated electrolyte, while a significant cathodic peak of all catalysts is clearly observed in the O_2-saturated solution. Obviously, the Fe-NC-3 catalyst presents a high ORR activity, which is approaching Zn-NC-3 (Figure S4b and Figure S4c). Moreover, the Fe-NC-3 exhibits more positive peak potential than that of three nitrogen-doped carbon materials. It demonstrates that incorporating metal atoms into carbon material can improve ORR electrocatalytic activity in alkaline media.

3.2 LSV curves of Fe/Fe-NC-3.

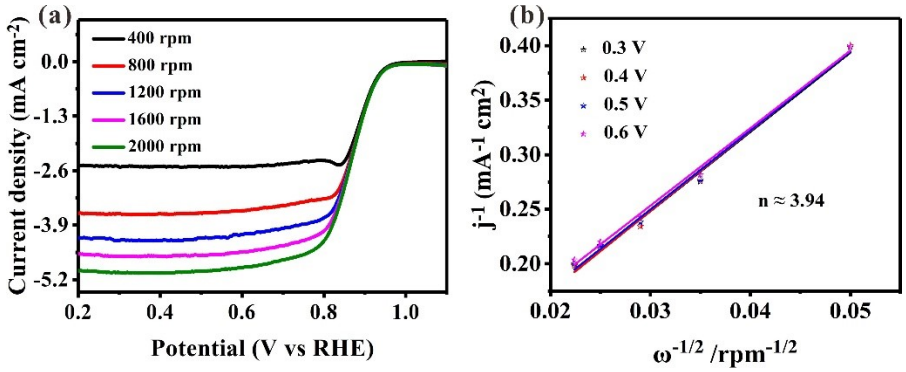

Figure S5. (a) LSV curves for Fe/Fe-NC-3 at various rotation rates. (b) The corresponding K-L plots at different potentials and the number of electron transfers calculated of Fe/Fe-NC-3.

From the slopes of the KL plots (inset of Figure 4c), the Fe/Fe-NC-3 shows the electron transfer number (3.94) in the potential range of (0.2 - 0.6 V), suggesting that the production of H_2O_2 is almost minimal. The H_2O_2 and Fe species can happen a Fenton reaction, leading to the reduction of Fe-Nx active sites and therefore an unsatisfactory stability performance.

3.3 ORR curves of Zn-NC-3 and Fe-NC-3 at 1600 rpm.

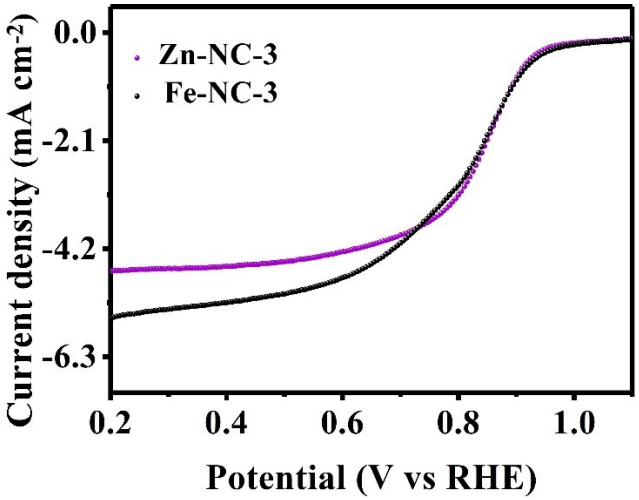

Figure S6. ORR curves of Fe-NC-3 and Zn-NC-3 in 0.1 M aqueous KOH.

As revealed in the LSV curves (Figure S6), the Fe-NC-3 demonstrates a higher limiting diffusion current density than Zn-NC-3 catalysts. Moreover, the E_{onset} of Fe-NC-3 is 0.94 V, approaching the corresponding values of Zn-NC-3.

3.4 C_{dl} of as-synthetic materials.

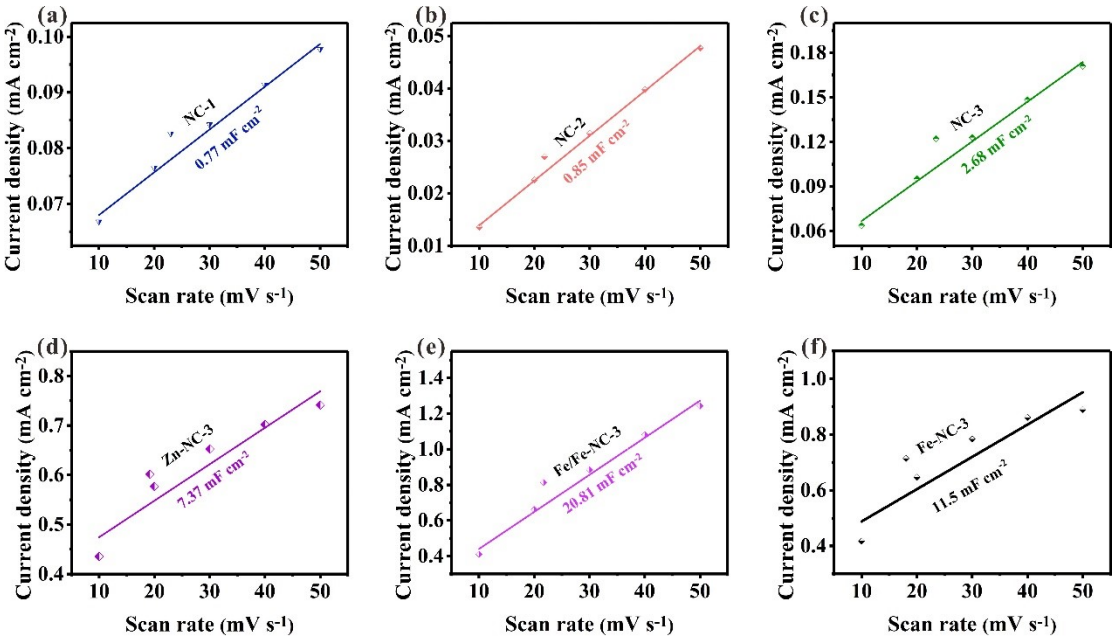

Figure S7. (a-f) Calculated C_{dl} of NC-1, NC-2, NC-3, Zn-NC-3, Fe/Fe-NC-3, and Fe-NC-3 in 0.1 M KOH.

The C_{dl} value of the sponge structure (Fe/Fe-NC-3) is 20.81 mF cm^{-2} much higher than that of the as-synthesized sample, indicating that Fe/Fe-NC-3 exposures more surface sites for chem-adsorption/desorption of reactants and subsequent reactions.

3.5 OER polarization curves.

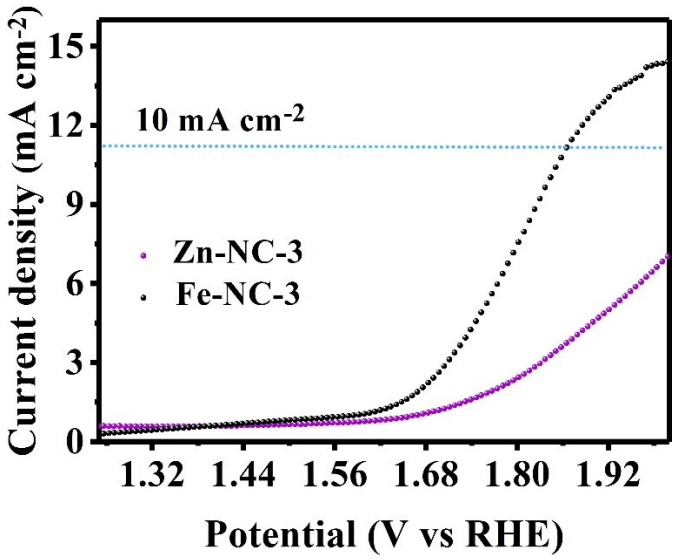

Figure S8. OER curves of Zn-NC-3 and Fe-NC-3 in 1 M aqueous KOH.

3.6 Schematic representation of primary ZAB.

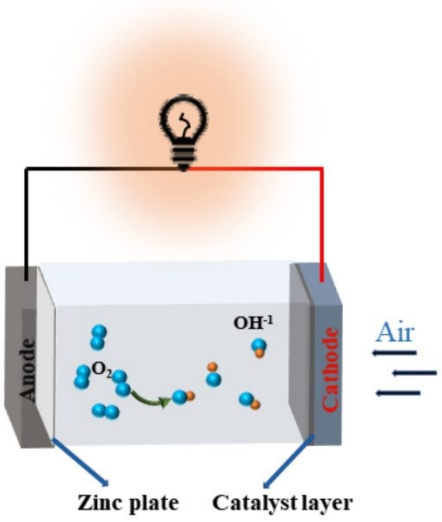

Figure S9. Schematic representation of primary of ZAB.

As can be seen in Figure S9, homemade aqueous rechargeable ZABs are assembled using Zn foil as the anode, Fe/Fe-NC-3 as the air cathode catalyst, and 6.0 M KOH + 0.2 M $Zn(CH_3COO)_2$ as the electrolyte.

3.7 Electrochemical performances of these electrode materials.

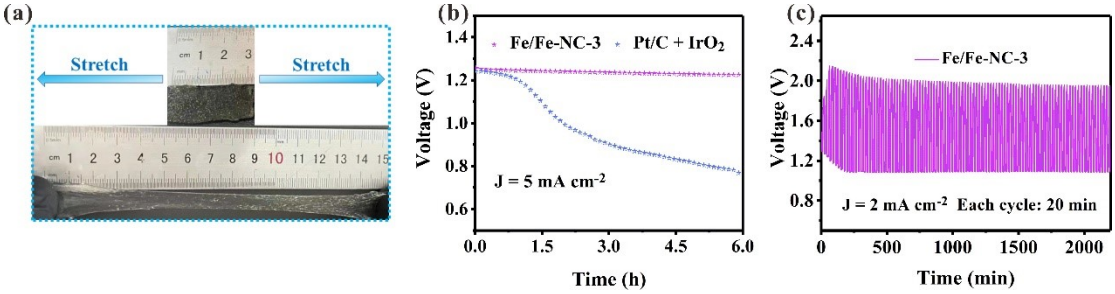

Figure S10. (a) Optical pictures of PVA electrolyte in the original state, tensile state, and compression state. (b) Long-time discharge curves of Fe/Fe-NC-3 at 5 mA cm^{-2}. (c) Galvanostatic discharge and charge cycling performance of Fe/Fe-NC-3-based flexible ZABs with each cycle for 20 min at 2 mA cm^{-2}.

The PVA hydrogel electrolyte is easily stretched and completely recovered to its original location without any visible cracking, establishing its outstanding mechanical property and alkaline tolerance (Figure S10a). Under a constant discharge current density of 5 mA cm^{-2}, the flexible ZABs with Fe/Fe-NC-3 cathode can retain the original discharge voltage without the obvious potential drop in Figure S10b. The cycle stability tests of the catalyst battery are conducted via continuous discharging/charging at 2 mA cm^{-2}. As described in Figure S10c, the Fe/Fe-NC-3 electrode exhibits high cycling stability of 110th cycles without distinct round-trip overpotential change.

Table S1. Comparison of electrocatalytic performances between Zn-NC/GD sample and recently reported electrocatalysts applied in Zn-air batteries.

Catalyst	Electrolyte (6.0 M KOH+X)	Specific capacity (mAh g_{zn}^{-1})	Power density (mW cm^{-2})
Fe/Meso-NC-1000[6]	X = 0.2 M Zn $(Ac)_2$	/	109.6
FePc&rGo[7]	X = 0.2 M Zn $(Ac)_2$	739.7	103.0
SA-Fe-3DOMC[8]	X = 0.2 M Zn $(Ac)_2$	786.6	140.0
AA-Fe2N@NC[9]	X = 0.2 M Zn $(Ac)_2$	/	168.1
N-GCNT/FeCo[4]	X = 0.2 M Zn $(Ac)_2$	872.2	97.6
Fe_3C@NPW[10]	X = 0.2 M Zn $(Ac)_2$	804.4	78.0
Fe-SCNC[11]	X = 0.2 M Zn $(Ac)_2$	/	163.0
Fe/Fe-NC-3[This work]	X = 0.2 M Zn $(Ac)_2$	**812.2**	**304.4**

References

1. D. Wu, B. Ni, Y. Liu, S. Chen and H. Zhang, *J. Mater. Chem. A*, 2015, **3**, 9645-9657.

2. L. Zhang, Y. Long, Z. Chen and M. Wan, *Adv. Funct. Mater.*, 2004, **14**, 693-698.

3. Z. Liu, X. Zhang, S. Poyraz, S. P. Surwade and S. K. Manohar, *J. Am. Chem Soc.*, 2010, **132**, 13158-13159.

4. C.-Y. Su, H. Cheng, W. Li, Z.-Q. Liu, N. Li, Z. Hou, F.-Q. Bai, H.-X. Zhang and T.-Y. Ma, *Adv. Energy Mater.*, 2017, **7**, 1602420.

5. D. Guo, R. Shibuya, C. Akiba, S. Saji, T. Kondo and J. Nakamura, *Science*, 2016, **351**, 361-365.

6. S.-N. Zhao, J.-K. Li, R. Wang, J. Cai and S.-Q. Zang, *Adv. Mater.*, 2022, **34**, 2107291.

7. Z.-y. Mei, S. Cai, G. Zhao, Q. Jing, X. Sheng, J. Jiang and H. Guo, *Energy Storage Mater.*, 2022, **50**, 12-20.

8. P. Li, X. Qi, L. Zhao, J. Wang, M. Wang, M. Shao, J. S. Chen, R. Wu and Z. Wei, *J. Mater. Chem A*, 2022, **10**, 5925-5929.

9. A. Zhu, L. Qiao, P. Tan, Y. Ma, W. Zeng, R. Dong, C. Ma and J. Pan, *Appl. Catal. B: Environ.*, 2019, **254**, 601-611.

10. M. Cao, Y. Liu, K. Sun, H. Li, X. Lin, P. Zhang, L. Zhou, A. Wang, S. Mehdi, X. Wu, J. Jiang and B. Li, *Small*, 2022, **18,** 220201.

11. L. Zou, C.-C. Hou, Q. Wang, Y.-S. Wei, Z. Liu, J.-S. Qin, H. Pang and Q. Xu, *Angew. Chem. Int. Ed.*, 2020, **59**, 19627-19632.